Hindawi
Structural Control and Health Monitoring
Volume 2024, Article ID 5960162, 17 pages
https://doi.org/10.1155/2024/5960162

Research Article

Nonlinear Response Characterization of Post-Tensioned R.C. Bridges through Hilbert–Huang Transform Analysis

Fabrizio Scozzese and Andrea Dall'Asta

School of Architecture and Design, University of Camerino, Ascoli Piceno, Italy

Correspondence should be addressed to Fabrizio Scozzese; fabrizio.scozzese@unicam.it

Received 2 November 2023; Revised 3 February 2024; Accepted 12 February 2024; Published 23 February 2024

Academic Editor: Lucia Faravelli

A novel methodology for the characterisation of the nonlinear behaviour of post-tensioned r.c. bridges, which exploits the response to heavy traffic travelling during operational conditions, is presented. This type of bridges shows a nonlinear elastic behaviour due to the partial opening of cracks under heavy loads whose entity is related to the intensity of the prestressing force. The properties of this response vary because of material relaxation or damage of the prestressing system. The study exploits the abilities of the Hilbert–Huang transform (HHT) to extract the instantaneous properties of the dynamic response, and a novel procedure to characterise the nonlinear elastic response is presented and investigated through theoretical applications on simplified dynamic systems. A frequency-amplitude correlation chart is proposed as a visual tool to retrieve useful information on the nonlinear response related to the instantaneous variation of the natural frequency with the response amplitude. With the aim of denoising and eliminating spurious contributions introduced by the local nature of the information extracted through the Hilbert spectral analysis, a probabilistic model is proposed for the result interpretation, through which the probability distribution of the instantaneous natural frequencies conditional to different levels of the response amplitude is provided and potential bridge's response modifications and anomalous behaviours of the prestressing system can be detected. An extensive parametric analysis is performed to assess the influence of the most relevant parameters governing the problem and verify the effectiveness of the proposed strategy.

1. Introduction

This study concerns the identification of mechanical properties of post-tensioned reinforced concrete (r.c.) structures. Such systems are prestressed by internal slipping tendons encapsulated within a protective sleeve and linked, only at a later stage, to the structure (after tendon tensioning) by in situ grouting injection of their encapsulating ducting. In this case, the main feature of interest is the entity of the prestressing force that controls the structure load capacity. Even though some of the following concepts can be used in many structural systems, this study is specifically oriented to the characterisation of prestressing forces acting on bridge decks consisting of parallel beams, connected by an upper r.c. slab. The one at hand is among the most diffused typologies built around the 70–80s in many countries [1–3]; the vulnerability of these bridges is quite high due to the level of degradation they are usually exposed to, in particular regarding the state of conservation of the precompression system (presence of humidity into the protective sleeves and corroded tendons) and to make things worse it shall be acknowledged that the healthy state of such components cannot be evaluated through visual inspection or conventional tests, but special inspections are needed [4–7]. This aspect strongly reflects on the reliability of these systems, which is notably influenced by the actual state of the cables, whose degradation gradually increases over time [8–10].

The prestressing force and the cable path are usually designed to limit the structure cracking under service conditions [11, 12], and the system response is essentially linear. In this case, a deviation from the linear response

arises only when the external loads attain high values, close to the maximum values considered in the design. Long-term rheological phenomena (concrete creep, concrete shrinkage, and steel relaxation), defects in the construction process, or steel corrosion of the cables provide a reduction in the prestressing force and a rise in the nonlinearity of the response under travelling loads. Cracking usually closes again once the load decreases and returns below a given threshold value. The system response can be classified as nonlinear elastic, and the transition between the initial stiffness and the reduced stiffness due to cracking is ruled by the intensity of the effective prestressing force.

The identification of the prestressing force and its monitoring over the time cannot be carried out exploiting low energy input methods, e.g., through operational modal analysis [13], because prestressing force does not affect the flexural stiffness in the linear response range, and a marginal influence can only be observed in more complex vibration modes (e.g., torsional modes), as widely demonstrated in theoretical and experimental studies ([14–18]).

The characteristics of the nonlinear behaviour of the system can be studied by exploiting the strong input produced by the passage of heavy trucks. This type of loads provides a dynamic response involving high displacements and relevant strain energy for a limited time duration. Heavy loads regularly travel over the bridge and a continuous monitoring is possible under service conditions. However, the travelling loads provide a nonstationary and nonlinear response; furthermore, the characteristics of the travelling load itself are generally unknown. Therefore, the analysis of data requires specific methods.

In the present study, the problem is approached by exploiting the abilities of the Hilbert–Huang transform (HHT) to extract the instantaneous property of vibration motions [19, 20], and this information is combined with the total displacements in order to characterise the nonlinear elastic response due to the prestressing force. In particular, the local motion consequent to a vehicle crossing the bridge generally consists of a carrier deformation history, which can be associated with the deformation produced by a quasi-static passage, and a further overlapped vibration motion related to the load velocity and the dynamic properties of the bridge, the latter depending on the instantaneous stiffness varying with the current total deformation. The HHT makes it possible to derive the instantaneous tangent stiffness from the instantaneous frequencies of vibration modes, and the correlation with measures depending on the total strain energy, e.g., displacement or curvature, allows us to recover the nonlinear elastic response.

In the last two decades, HHT was widely used in different contexts involving nonlinear and nonstationary system responses, and some applications were also developed for bridge analysis, with different objectives [21, 22]. A state of the art about the use of HHT in bridge engineering can be recovered in [20], and some more recent applications are reported in [23]. Only a few number of investigations were oriented to evaluate variations within the nonstationary response (see Chapters 14 and 15 of the book of Chen et al. [20]). These authors demonstrated the ability of HHT to extract instantaneous dynamic properties for bridge response, but they did not focus on the nonlinear relationship between the response and the prestressing force or other significant state variables, which is the core of the study presented in this paper.

However, the analysis of the outcomes of HHT is not trivial, because Hilbert transform provides quasi-local information that may show irregularities in time. In this study, a probabilistic model is proposed to analyse the nonlinear trend arising between instantaneous tangent stiffness and structural displacements. The model can be inferred from measures recorded during a number of passages of vehicles with significant mass and can be potentially used for anomaly detection even if the travelling load is unknown.

An extensive parametric analysis is performed in this paper on simple dynamic systems to assess the influence of the most relevant parameters governing the problem and verify the effectiveness of the proposed strategy. The paper is structured as follows: The adopted problem formulation concerning a nonlinear elastic beam response under travelling loads is presented in Section 2, the proposed methodology for the outcome analysis is described in Section 3, the method applications and related parametric investigations are presented in Section 4, and finally, the main conclusions are summarised in Section 5.

2. Problem Formulation

The dynamic response of bridges under travelling loads has been widely studied in the last decades ([24–28]).

Models for the response of a simply supported beam subjected to a single force moving with constant velocity can be recovered in [29–32], and the relevant solution for a linear system with constant mechanical properties along the beam is reported in [21]. This solution is obtained by a modal decomposition, and the first-mode contribution is generally dominant, at least for what concerns the midspan displacement, and the effects of structural damping are usually small.

In the following, a general formulation is presented, and the solution for a linear system with constant properties is recalled. Furthermore, the approximate solution for the nonlinear problem is presented. The latter will be used in the subsequent chapter for a parametric analysis, in order to study the response of single degree of freedom systems.

Let $x \in [0, L]$ be the variable identifying the points of a beam with length L, $t \in [0, \infty)$ denotes time, $u(x, t) \in U \times -[0, \infty)$ is the transverse displacement, and U is the functional space of possible beam deformations. Differential problem governing the beam motion consists of the following field equation complemented by proper initial and boundary conditions:

$$\begin{aligned} \ddot{u}(x,t) + c(x)\dot{u}(x,t) + \left(b\left(x;u''\right)u''(x,t)\right)'' &= p(x)\Delta(x-vt), \\ u(x,0) = \dot{u}(x,0) &= 0, \\ u(0,t) = u(L,t) = u''(0,t) = u''(L,t) &= 0, \end{aligned} \tag{1}$$

where primes and superposed dots denote spatial and time derivatives, respectively; Δ is the Dirac delta function; functions c and b are known potentially variables along the beam and describe dissipative properties and the ratio between bending stiffness and unit mass, respectively; p is the ratio between the travelling constant force and the unit mass, and v is the load velocity. It is assumed that the bending stiffness is nonlinear, and it is related to the curvature u''. The field equation describes the motion during the load travelling time $T = L/v$, and after that, free vibrations occur. The presented formulation is based on Euler–Bernoulli beam theory, and it is adequate to describe the response of slender beams where shear strain and rotational inertial term can be neglected [15].

For undamped linear response $c(x) = 0$ and constant beam properties $b(x,u'') = b_0$, analytical expressions of the vibration modes $\varphi_k(x)$ and vibration circular frequencies ω_k can be easily obtained:

$$\begin{aligned} \varphi_k(x) &= \frac{1}{2L}\sin\left(k\pi\frac{x}{L}\right), \\ \omega_k &= \frac{\pi^2 k^2}{L^2}\sqrt{b_0}, \end{aligned} \tag{2}$$

and the set of vibration modes provides a complete series of functions in the subspace $U_0 \subset U$ of u satisfying the boundary conditions. The weak formulation of the problem [33, 34] can be obtained multiplying the differential equations by the vibration modes and integrating by parts (dependence on x and t is understood):

$$\begin{aligned} &\langle \ddot{u}, \varphi_k\rangle + \langle c\dot{u}, \varphi_k\rangle + \langle b\left(u''\right), \left(\varphi_k\right)''\rangle = \langle p\Delta(x-vt), \varphi_k\rangle, \quad \forall k, \\ &u(x,0) = \dot{u}(x,0) = 0, \end{aligned} \tag{3}$$

where

$$\langle v, w\rangle = \int_0^L v(\xi)w(\xi)d\xi. \tag{4}$$

Vibration modes are orthonormal functions, i.e., $\langle \varphi_k, \varphi_j\rangle = \delta_{ij}$, with the Kronecker delta δ_{jk}. Approximate solutions can be obtained by assuming $u(x,t) = q_j(t)\varphi_j(x)$ (repeated index denotes summation) and considering a limited number of vibration modes $k = 1, \ldots, N$:

$$\begin{aligned} \ddot{q}_k + \widetilde{c}_{jk}\dot{q}_k + \widetilde{b}_k(q_1, \ldots, q_N) &= \widetilde{p}_k, \\ q_k(0) = \dot{q}_k(0) &= 0, \end{aligned} \tag{5}$$

where $\widetilde{c}_{jk} = \langle c\varphi_j, \varphi_k\rangle$ is a generalized damping term, $\widetilde{b}_k = \langle b(q_l(\varphi_j)''), (\varphi_k)''\rangle$ is a generalized stiffness term, and the loading term is as follows:

$$\widetilde{p}_k = \langle p\Delta(x-vt), \varphi_k\rangle = p\varphi_k(x-vt). \tag{6}$$

In the case of constant properties, only diagonal terms survive and the contributions related to each vibration mode can be studied separately. Analytical expressions are reported in [21]. Some results about this case are recalled: (i) the response is ruled by the speed ratios $S_k = k\pi v/\omega_k L$ between the circular frequency associated with the moving load and the beam vibration circular frequencies; (ii) the effect of damping of bridges is marginal; (iii) the contribution of higher modes can be neglected at the midspan section of the beam. So, a single-degree-of-freedom model is often used in the problem analysis when the midspan deflection only is of interest. In the following investigation, results concerning the nonlinear response of the system will be considered, and a single-degree-of freedom system is studied by considering the first term only on the series φ_k. A preliminary study was carried out to verify if previous conclusions hold in the nonlinear case, within the range of stiffness variations of interest: the comparison of solutions considering only the first term with solutions involving more terms, and more vibration modes, confirmed previous statements in the range of interest. The single-degree-of-freedom model reduces to

$$\begin{aligned} \ddot{q} + \widetilde{c}\dot{q} + \widetilde{b}(q) &= \widetilde{p}, \\ q(0) = \dot{q}(0) &= 0. \end{aligned} \tag{7}$$

3. Proposed Methodology

The methodology proposed in this paper exploits the capability of the Hilbert–Huang Transform (HHT) in extracting the instantaneous features of the vibration motion of a dynamic system (e.g., the bridge deck or simply a beam) [19]. In particular, the local motion induced by the passage of a vehicle is of interest here, which produces a nonlinear and nonstationary deformation time history on the system that

can be seen as the combination (superposition) of a deformation produced by a quasi-static transit, whose entity depends on the moving load weight, and a series of vibration motions depending on the moving load velocity and the dynamic properties of the bridge, the latter depending itself on the committed instantaneous stiffness.

The idea presented in this study is that of exploiting HHT to evaluate the instantaneous frequencies (varying due to nonlinear response) of the system (from the dynamic vibration mode characterising the bridge response) and to correlate them with a measure depending on the total strain energy (displacements are used in this work, but other quantities, e.g., the curvature, could be used) in order to recover information on the current nonlinear elastic response. It is underlined that instantaneous frequencies or, more precisely, the derivatives of the phase angles are directly related to the instantaneous tangent stiffness (e.g., $d\tilde{b}(q)/dq$), the latter being a sensitive parameter that makes it possible to fully recover the nonlinear behaviour of the system once it is correlated to a strain measure (e.g., q). This way, the nonlinear behaviour under heavy traffic can be recovered even if the travelling load is unknown.

However, the analysis of the outcomes of HHT is not trivial, because Hilbert transform provides quasi-local information that may show irregularities in time. In this study, a probabilistic model is proposed to estimate the modal frequencies conditional to different displacement levels. The model can be inferred from measures recorded during a number of passages of vehicles with significant mass and can be used for the subsequent nonlinear response identification.

The methodology, qualitatively defined above, requires different tools to be performed which can be summarised as in the following four points, further detailed individually in the next subsections:

(i) Empirical mode decomposition (EMD), required to extract the vibrational component of the motion carrying information on the system dynamic properties;

(ii) Hilbert transform of the extracted dynamic component of the motion, required to enrich the signal with its imaginary part, permitting the extraction of the instantaneous properties of the motion;

(iii) Correlation between the instantaneous frequencies and the simultaneous response displacement within a chart providing information on the system's response nonlinearity;

(iv) Construction of a probabilistic model inferred from the data of step iii, useful to ease the results' interpretation and the identification of nonlinear patterns of the response.

The combination of tools i and ii, i.e., the empirical mode decomposition and the Hilbert spectral analysis, is also known in the literature as the "Hilbert–Huang transform" (HHT) and actually represents a signal processing technique developed by Norden E. Huang in the late 1990s [35] for analysing signals with rapidly varying frequency components or those with abrupt changes in amplitude, in other words nonstationary and nonlinear signals.

3.1. Empirical Mode Decomposition (EMD). The empirical mode decomposition (EMD), originally proposed by Huang et al. in 1998 [35], consists of a "sifting and averaging" procedure through which any nonlinear and nonstationary signal $y(t)$ can be adaptively decomposed into a number of intrinsic mode functions (*IMFs*) $\eta_k(t)$, without the need of a priori basis as for Fourier and Wavelet-based methods:

$$y(t) = \sum_k \eta_k(t). \tag{8}$$

The advantage of such decomposition for the purposes of the present application lies in the fact that each extracted IMF is a monocomponent amplitude- and frequency-modulated signal [36], and thus, unlike the original signal, it is characterised by a monotonically increasing phase and a positive instantaneous frequency, which represent necessary conditions for a correct estimation of the local dynamic features via the subsequent application of the Hilbert transform (see next subsection). In order to be classified as IMF, the identified subcomponents shall satisfy two criteria: (1) within the whole time series, the number of extrema and the number of zero crossings shall be either equal or differ at most by one; (2) at any point in the time series, the mean value of the upper envelope made by the local maxima and the lower envelope formed by the local minima must be equal to zero (i.e., the upper and lower envelopes are locally symmetrical with respect to the time axis).

A visual example of the outcomes provided by the EMD procedure in the case of the response of a bridge under a travelling load is given in Figure 1, where the sifting process is applied to the response deflection time history of an elastic beam subject to a punctual load travelling with constant velocity: The original signal is shown on the top, then, the identified oscillatory modes are sorted top-down from the highest to the lowest frequency content, so that in this case, IMF 1 represents the dynamic oscillatory component (the useful part for extracting local information on the system response), IMF 2 represents the quasi-static component (which can be neglected for the purposes of the nonlinear identification method proposed in this study), and the residual is shown on the bottom of the chart.

3.2. Hilbert Transform (HT). The Hilbert transform $H[y(t)]$ (HT), applied to a generic signal $y(t)$, provides the function $h(t)$ (Eq. (9)):

$$h(t) = \frac{PV}{\pi} \int_{-\infty}^{\infty} \frac{y(\tau)}{t-\tau} d\tau, \tag{9}$$

(PV being the Cauchy principal value of the integral) containing the previously missing imaginary part ($ih(t)$) of the original signal $y(t)$, necessary to have a more complete description through the new complex signal $z(t)$:

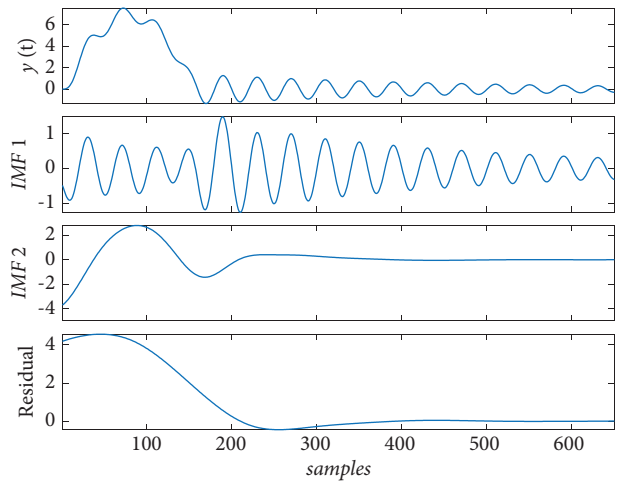

FIGURE 1: EMD applied to the response deflection time history of an elastic beam under travelling load with constant velocity.

$$z(t) = y(t) + ih(t) = r(t)e^{i\theta(t)}, \tag{10}$$

where i is the imaginary unit, $r(t)$ is the modulus (radius of rotation) and $\theta(t)$ is the phase angle:

$$r(t) = \sqrt{y^2(t) + h^2(t)},$$
$$\theta(t) = \arctan\left(\frac{h(t)}{y(t)}\right). \tag{11}$$

The information extracted through HT is fundamental to recovering the local information about the system response during the passage of a vehicle; indeed, the instantaneous circular velocity $\omega(t)$ can be derived through differentiation of the phase angle:

$$\omega(t) = \frac{d\theta(t)}{dt}, \tag{12}$$

and, if the signal represents an oscillation, it can be interpreted as an instantaneous natural circular frequency (hereinafter referred to as instantaneous frequency or simply frequency). In this regard, it must be noted that the direct application of the HT to the original multifrequency signal (e.g., the recorded monitored quantity $y(t)$) would only provide misleading instantaneous frequencies, which may show unphysical negative values over the time [37]. This is the reason why HT must be applied to the IMFs extracted via the EMD procedure and more precisely to the specific component of vibration carrying information on the system dynamic response (depicted with red lines in the example of Figure 2, providing a representation of the original signal $y(t)$ and its dynamic first oscillatory component IMF 1 in both the (a) time domain and (b) complex plane).

3.3. Frequency-Amplitude Correlation Charts. Once the instantaneous circular frequencies have been evaluated, the data are correlated with a proper response measure; for instance, the displacement or curvature amplitudes represent suitable choices being state variables directly related to the total strain energy.

A frequency-amplitude correlation chart is thus provided to highlight potential changes in the circular frequencies $\omega(t)$ (it is recalled that ω^2 is proportional to the tangent stiffness of the system) with the amplitude of the response (midspan displacements are used in this work as response measures), allowing us to recover information on the nonlinear elastic response of the system.

In Figure 3, a frequency-amplitude correlation chart is shown with illustrative purposes, where the typical responses of a linear (red plots) and nonlinear (blue plots) elastic beam subjected to the passage of a heavy vehicle travelling with constant velocity are compared. The nonlinear elastic response is ruled by a bilinear model in which the natural frequency values related to first and second branch are denoted as ω_0 and ω_1, respectively, and they are represented by dashed horizontal lines in the figure. This chart contains useful information about the behaviour of the systems and highlights the unsymmetrical response nonlinearity (where present) associated, in this example, with the highest positive displacements.

3.4. Probabilistic Model. In general, the analysis of the outcomes of HHT is not trivial, because Hilbert transform provides quasi-local information that may trace irregular paths. This reflects on the results presented in the previous chart (Figure 3) which might be not of immediate understanding, and useful information on the bridge response might consequently remain hidden. To cope with this issue, in this study, a probabilistic model is inferred from the problem output to analyse the general trend of the response, including local irregularities coming from the transform. The probabilistic model provides the distribution of the modal frequencies conditional to the displacement level.

In more detail, it is assumed that pairs (ω, y) are the samples of random variables (Ω, Y), whose statistical properties are described by the conditional probability density function (PDF) $f_{\Omega|Y}(\omega \mid y; \mathbf{p})$, and related characteristic parameters are collected in the vector $\mathbf{p}$; the latter can be inferred from an available set of data pairs (ω_m, y_m) $(m = 1..N)$. The model parameters are evaluated by means of the maximum likelihood method, assuming the following log-likelihood objective functions $L_{\ln}(\mathbf{p})$ [38–40]:

$$L_{\ln}(\mathbf{p}) = \sum_m \ln\left[f_{\Omega|Y}(\omega_m|y_m; \mathbf{p})\right], \tag{13}$$

where the pairs (ω_m, y_m) denote the m^{th} data observation from which the model provides the corresponding probability of occurrence.

For the aim of the present work, a normal Gaussian model is adopted, but other shape functions could be used to describe the conditional PDF, provided that they satisfy the conditions of positive definiteness and unitary integral along ω for each y.

The two coefficients characterising the PDF, i.e., the mean μ and the standard deviation σ of the distribution, are assumed to vary with the response amplitude according to the following equations:

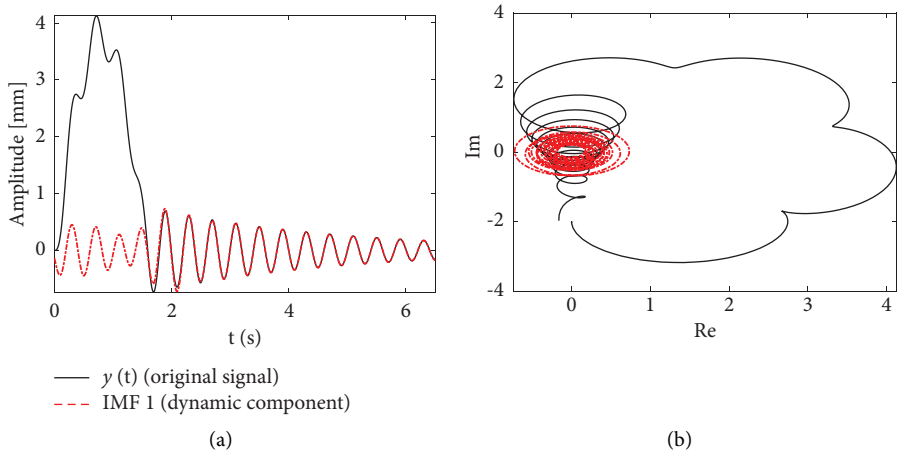

FIGURE 2: Original signal and its dynamic first oscillatory component: (a) time domain and (b) complex plane representation.

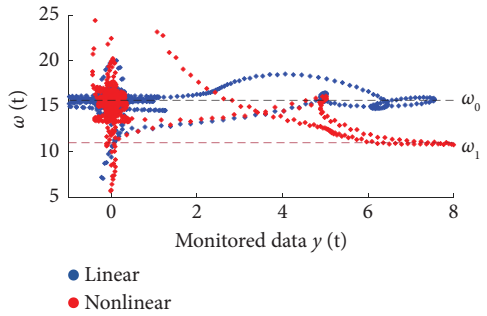

FIGURE 3: Example of frequency-amplitude correlation chart: responses of linear and nonlinear elastic beam subjected to heavy moving loads.

$$\mu(y, \mathbf{p}^{\mu}) = p_1^{\mu} + \frac{p_2^{\mu}}{1 + e^{-(y - p_3^{\mu})}}, \tag{14}$$

$$\sigma(y, \mathbf{p}^{\sigma}) = p_1^{\sigma} + y p_2^{\sigma}, \tag{15}$$

with the model parameters collected in the vector $\mathbf{p} = [\mathbf{p}^{\mu}, \mathbf{p}^{\sigma}]$. The shape function adopted to describe the mean trend over the response amplitude y (equation (14)) is a three-parameter sigmoid function, which is suitable to describe behaviours characterised by the transition between two constant slope branches and is able to catch the main features of the patterns shown by the response data; the variance is assumed to vary linearly with the response (equation (15)).

For the sake of clarity, the exemplificative chart presented above in Figure 3 is now reproposed in Figure 4(a), where the $\mu(y)$ and $\mu(y) \pm \sigma(y)$ functions of the reference probabilistic model are superimposed on the data with solid and dashed lines, respectively (colours are pertinent to the case of analysis); on the right side of the figure, the PDFs of the instantaneous frequency conditional to four levels (see vertical dotted lines in the left plot) of the monitored quantity are presented. It can be observed how the probabilistic model provides a suitable tool to be used for a clearer and faster extraction of information about the variations of the local dynamic properties with the response amplitude. The nonlinear response and the transition of the system from the branche with high stiffness to the branch with low stiffness can be easily identified from these results.

4. Method Application and Parametric Analysis

An extensive parametric investigation is performed to assess the effectiveness of the proposed methodology in determining the nonlinear response of a bridge structure under travelling loads. A single-degree-of freedom model of a real precast bridge is studied by using the analytical formulation presented in Section 2, focusing on the midspan deflection response under the passage of moving loads with constant velocity. The first term $\varphi_1(x) = \sqrt{2/L}\sin(\pi x/L)$ of the orthonormal sinusoidal series has been used for the numerical solution, and the deflection at the midspan $x = L/2$ is $a(t) = u(L/2, t) = \sqrt{2/L}q(t)$ has been evaluated. The dynamic problem at hand has been numerically solved by the 4th order Runge–Kutta method [41], implemented within the MATLAB software [42].

First, a case study with a reference set of parameters is analysed to present the applicability of the method. Then, the influence of the parameters governing the problem is analysed by changing parametrically each term one by one in a range of meaningful values, in order to assess the effectiveness of the proposed methodology under various scenarios and conditions.

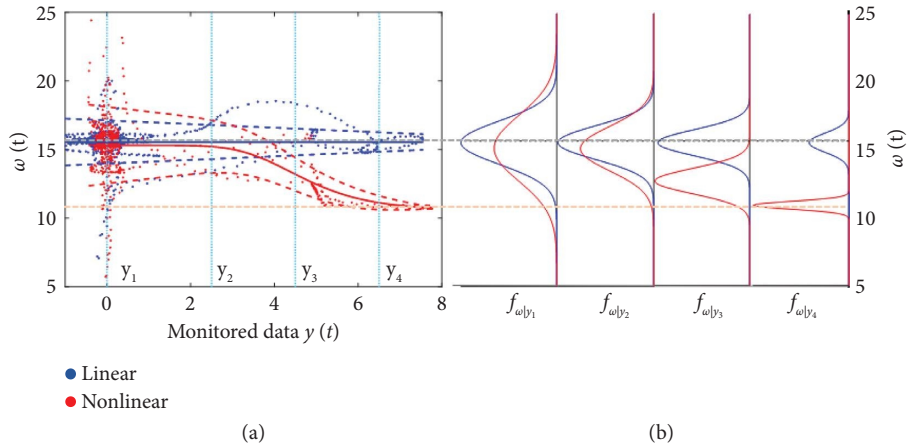

FIGURE 4: Probabilistic model built on through the data extracted from HHT (a) and PDFs of the instantaneous frequency conditional to four levels of monitored quantity (b).

The section is concluded with an application considering three traffic sequences as input rather than a single moving load (Subsection 4.6).

4.1. Reference Case Study

4.1.1. System Properties. A single-degree-of freedom system is derived from the formulation presented in Section 2 considering the first term of the analytical expression of the vibration modes, according to the reasons illustrated before. The system properties, assumed to be representative of the linear response of real precast bridges and able to provide realistic responses, are as follows: span length $L = 35.0$ m, elastic modulus $E = 35 \cdot 10^6$ kN/m^2, inner damping ratio $\xi = 2\%$, inertial moment $J = 1.62$ m^4, area $A = 6.0$ m^2, and material density $\rho = 2500$ kg/m^3 (mass per unit length $m = 15000$ kg/m). The cross-section properties are reported in Figure 5, and the characteristic ratios EJ/GAL^2 and J/AL^2, relevant to shear deformability and rotational inertial contribution, respectively, are negligible and confirm that the model presented in Section 2 is adequate for the problem at hand.

The system is assumed to respond according to a bilinear elastic force-displacement law (Figure 6), where the threshold of the response amplitude (midspan deflection) governing the passage from the first to the second elastic branch is equal to $a^* = 5.5$ mm and the stiffness ratio is $k_1/k_0 = \omega_1^2/\omega_0^2 = 0.60$, with k_0 and k_1 identifying the first and second elastic stiffness, respectively.

As long as the system deflection maintains lower than a^*, the first natural frequency of the bridge is $\omega_0 = 15.66$ rad/s (period $T_0 = 0.40$ s) and the tangent stiffness is constant and proportional to ω_0^2; the reduced natural frequency characterising the response in the second elastic branch is $\omega_1 = 12.13$ rad/s, i.e., $T_1 = 0.52$ s. This can be considered representative of the response of a healthy prestressed beam under service loads close to the maximum values considered in the design.

Concerning the moving vehicle properties, a realistic condition compliant with most of the National Highway Codes to date in force in Europe [7, 43] is considered, i.e., an heavy truck with a mass equal to 44.8t (maximum allowed mass, weight $P = 440$ kN) travelling at a (maximum allowed, constant) velocity $v = 80$ km/h. The frequency associated with the moving loads is $\omega_v = 1.99$ rad/s, and the corresponding speed parameter is $S = 0.1270$.

The response of the system to all the set of parameter values presented above is analysed in next Subsection 4.1.2; then, with the aim of assessing the influence of the main parameters and the effectiveness of the proposed methodology under various scenarios and conditions, a parametric investigation is performed on a relevant subset of parameters, i.e. $\{a^*, k_1/k_0, P, S\}$ (each parameter is varied one by one keeping the other fixed at the aforesaid reference values).

4.1.2. Reference Results. The response time history of the deflection experienced by the structural system ($k_1/k_0 = 0.60$, $a^* = 5.5$ mm) under the moving load ($P = 440$ kN, $v = 80$ km/h) is shown in Figure 7(a), with the threshold a^* identifying the elastic state transition represented by an horizontal dashed line. It can be seen as this limit is only exceeded for a small fraction of the travelling time (around 0.4 s), the latter being equal to 2.53 s (note that the analysed time window is 6.3 s long because the tail of the signal contains also the damped free vibration response of the system).

By applying the method described in Section 3, the instantaneous frequency can be extracted and correlated to the corresponding response amplitudes, providing the plot of Figure 7(b). A black-dashed horizontal line identifies the expected value of the frequency $\omega_0 = 15.66$ rad/s. To ease the result interpretation, a Gaussian probabilistic model is built on the data according to the procedure detailed in Subsection 3.4: the sigmoid-shaped median trend of the model is superimposed to the data through a continuous blue line, and the dispersion (median ± standard deviation) is shown by dashed blue lines.

Exploiting this model, information about the changes of the instantaneous frequency can be inferred at any amplitude value of interest, as shown in Figure 8 (charts from *a* to *f*) where the PDFs conditional to a set of increasing amplitude values (identified by vertical light blue-dotted lines in Figure 8) are presented. From the inspections of these PDFs, the following points can be observed:

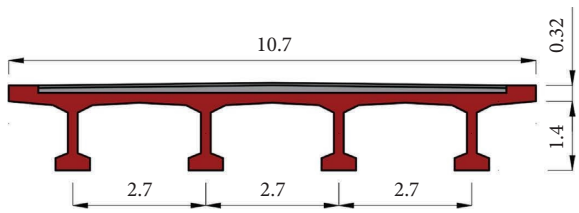

FIGURE 5: Bridge cross-section properties.

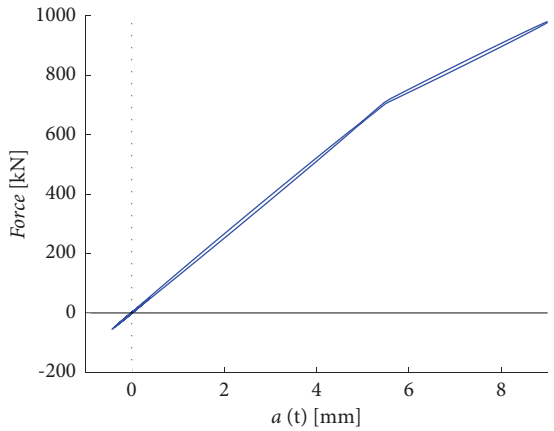

FIGURE 6: Bilinear elastic force-displacement law.

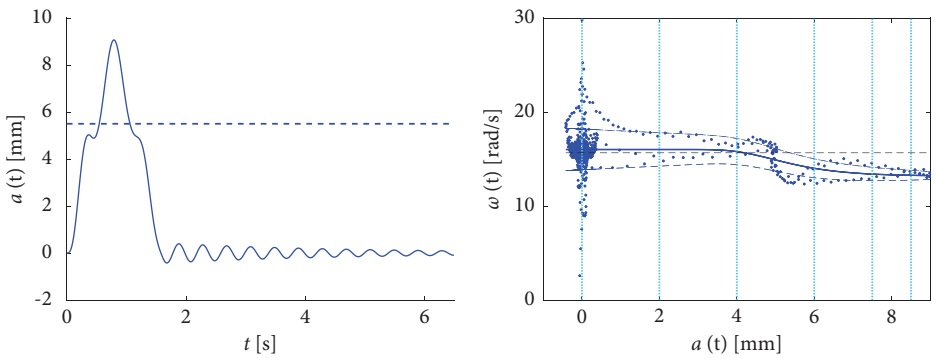

FIGURE 7: (a) Response time histories of the deflection amplitude; (b) frequency-amplitude correlation chart with the superimposed mean and variance of the probabilistic model.

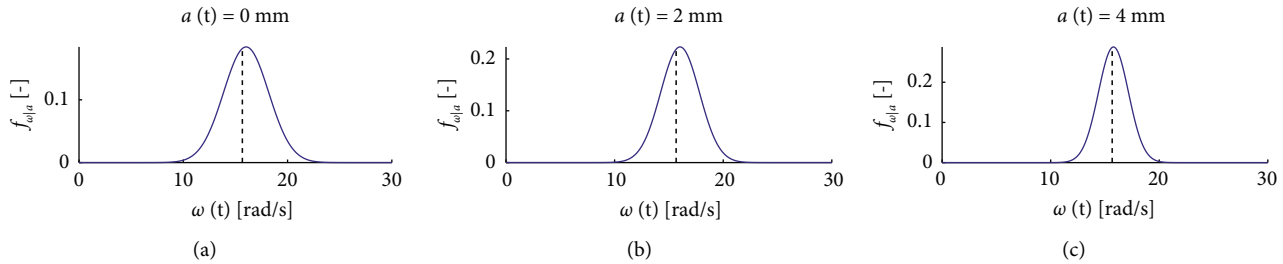

FIGURE 8: Continued.

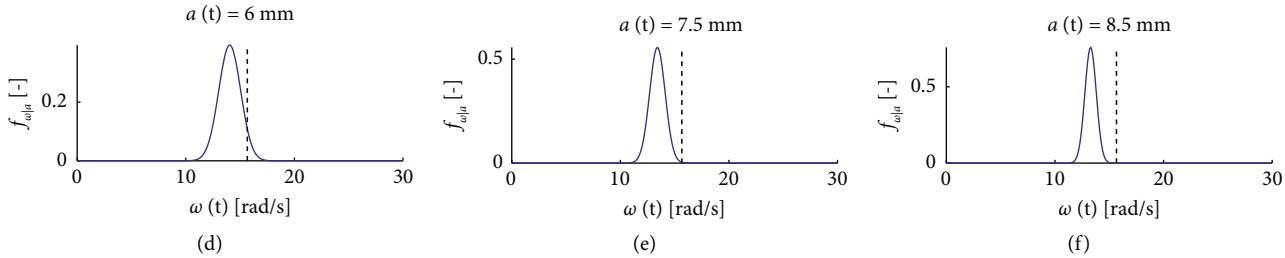

Figure 8: Instantaneous frequency distributions conditional to increasing levels of the response amplitude.

(i) for low response amplitude values, the instantaneous frequency remains, on average, approximately constant and equal to the expected value ω_0 (i.e., the PDFs are centered on ω_0);

(ii) for rising displacements, the instantaneous natural pulsations reduce below ω_0 and tend to stabilize on the value ω_1 for $a > a^* = 5.5$ mm;

(iii) the probabilistic model notably helps the graphical visualization of such nonlinear pattern of the frequency-amplitude response;

(iv) also, the dispersion of the instantaneous frequencies shows some degree of variability with the amplitude; in particular, it can be observed that values of σ decrease passing from small to high displacements;

(v) the method is suitable to catch the response nonlinearity and its unsymmetrical features (i.e., nonlinearity only occurs for positive deflection values).

4.2. Sensitivity to the Threshold Amplitude Governing the Nonlinear Elastic Transition. In this section and in the following sections, the sensitivity of the outcomes to variations of the nonlinear response is investigated. Variations in the prestressing force can be due to different long-term causes, such as the stress reduction due to concrete creep, concrete shrinkage, and or relaxation of the cables' steel, or they can be due to steel corrosion. These phenomena usually provide the variations of the threshold separating the first branch of the nonlinear response from the second branch, as well as the reduction of the stiffness of the second branch. The two variations are separately investigated, and in this section, the influence of the threshold value characterising the stiffness change in the bilinear response of the bridge is investigated. The following three values of a^* are analysed (Figure 9): 4.0 mm, 5.5 mm, and 7.0 mm (in terms of forces, these transitions occur at 50%, 70%, and 90% of the maximum force). The remaining system and vehicle parameters are kept fixed at the reference values ($P = 440$ kN, $v = 80$ km/h, and $k_1/k_0 = 0.60$).

The response time histories of the deflection experienced by the three structural systems under the same moving load are shown in Figure 10(a), while in Figure 10(b), the frequency-amplitude correlation chart is presented for all the analysed cases. The PDFs of the instantaneous frequency conditional to the amplitudes are provided in Figure 11. The same comments furnished for the previous case studies can be applied to the current outcomes, with the following two additional notes:

(i) the method is able to highlight the different nonlinear responses, and the threshold a^* affects the rapidity of the transition from the initial frequency ω_0 to the reduced frequency ω_1; indeed, the frequencies start changing later (higher response values) for higher thresholds a^*;

(ii) the threshold a^* has no influence on the entity of the frequency modifications, being the slope of the second elastic range equal in all the three analysed cases, and thus, all the PDFs tend to shift toward the same minimum reduced frequency value ω_1;

(iii) it is finally observed that even with very low levels of nonlinearity (as characterised by the case of $a^* = 7.0$mm), the proposed tool is capable of detecting the effects induced on the instantaneous frequencies, as testified by the frequency shift observed on the PDFs conditional to the highest displacements.

4.3. Sensitivity to the Levels of Nonlinearity. The influence of various levels of nonlinearity is now investigated by considering three values of the system stiffness ratio k_1/k_0 (Figure 12): 40%, 60%, and 80%. The other system and vehicle properties are kept fixed at the reference values ($P = 440$ kN, $v = 80$ km/h, and $a^* = 5.5$ mm).

In Figure 13(a), the response time histories are compared; in Figure 13(b), the frequency-amplitude correlation chart is presented, and the PDFs of the instantaneous frequency conditional to the response amplitudes are provided in Figure 14.

Also in this case, the method makes it possible to identify differences in the nonlinear response.

The outcomes show how the different stiffness ratios k_1/k_0 mainly affect the entity of the instantaneous frequency reduction. Indeed, different k_1/k_0 ratios correspond to different values of the reduced frequency ω_1. No significant shifts of the conditional PDFs are observed for response amplitudes $a < a^*$, while beyond this threshold, it can be seen how the lower the k_1/k_0 ratio, the higher the frequency reductions.

4.4. Sensitivity to the Speed Ratio. In this section, the ability of the method to identify the nonlinear response within the typical range of travelling velocities is investigated, considering different values of the speed parameter S (defined as the ratio of half the driving frequency to the bridge frequency, see Section 2). This is of interest because the maximum displacement does not rise proportionally with the velocity, not even in the linear

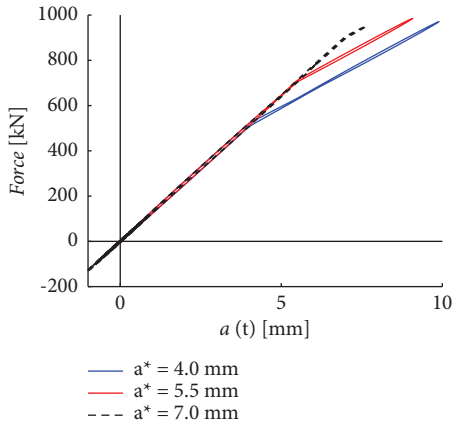

FIGURE 9: Bilinear elastic force-displacement laws for three values of a^*.

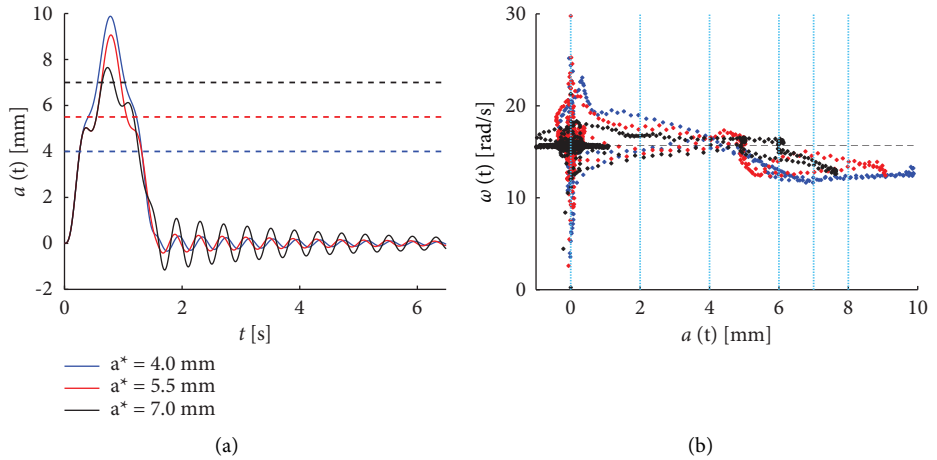

FIGURE 10: (a) Response time histories of the deflection experienced by the systems with different threshold values a^*; (b) frequency-amplitude correlation chart.

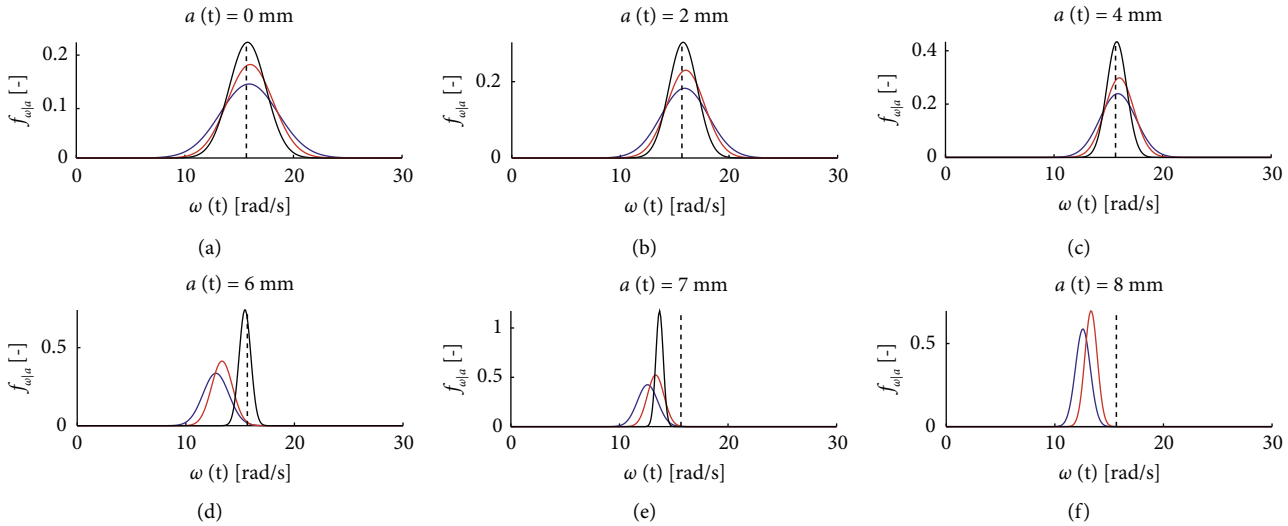

FIGURE 11: Instantaneous frequency distributions conditional to increasing levels of the response amplitude; comparison of systems with different a^*: 4.0 mm, 5.5 mm, and 7.0 mm.

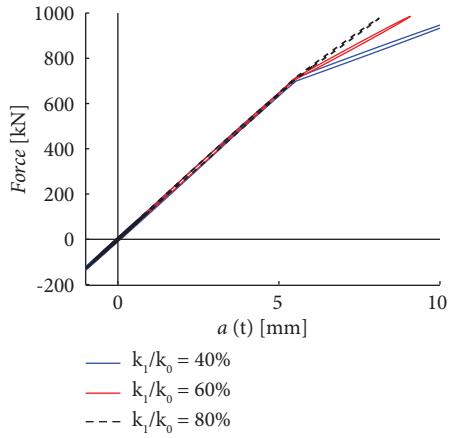

FIGURE 12: Bilinear elastic force-displacement laws with different stiffness ratios k_1/k_0.

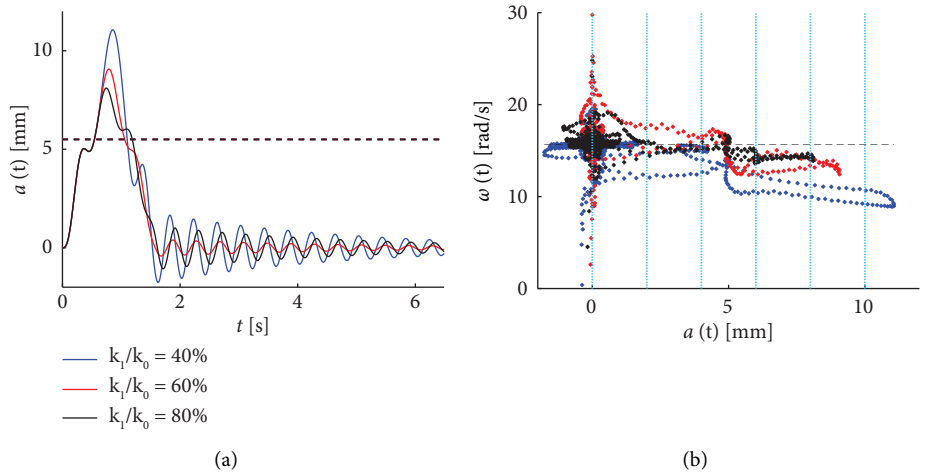

FIGURE 13: (a) Response time histories of the deflection experienced by the systems with different stiffness ratio k_1/k_0; (b) frequency-amplitude correlation chart.

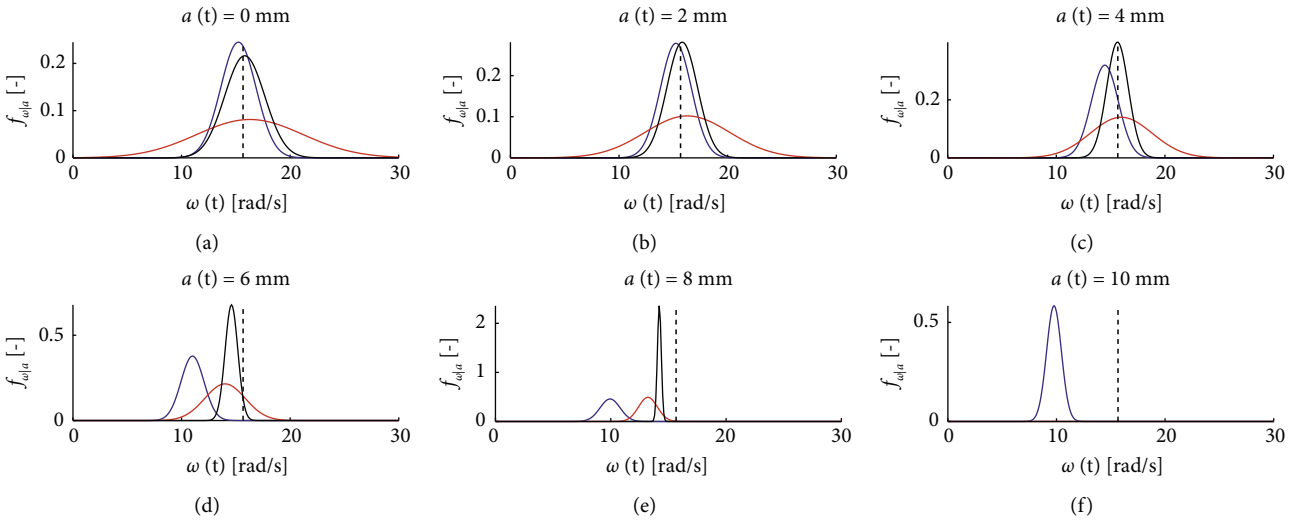

FIGURE 14: Instantaneous frequency distributions conditional to increasing levels of the response amplitude; comparison of systems with different ratios k_1/k_0: 40%, 60%, and 80%.

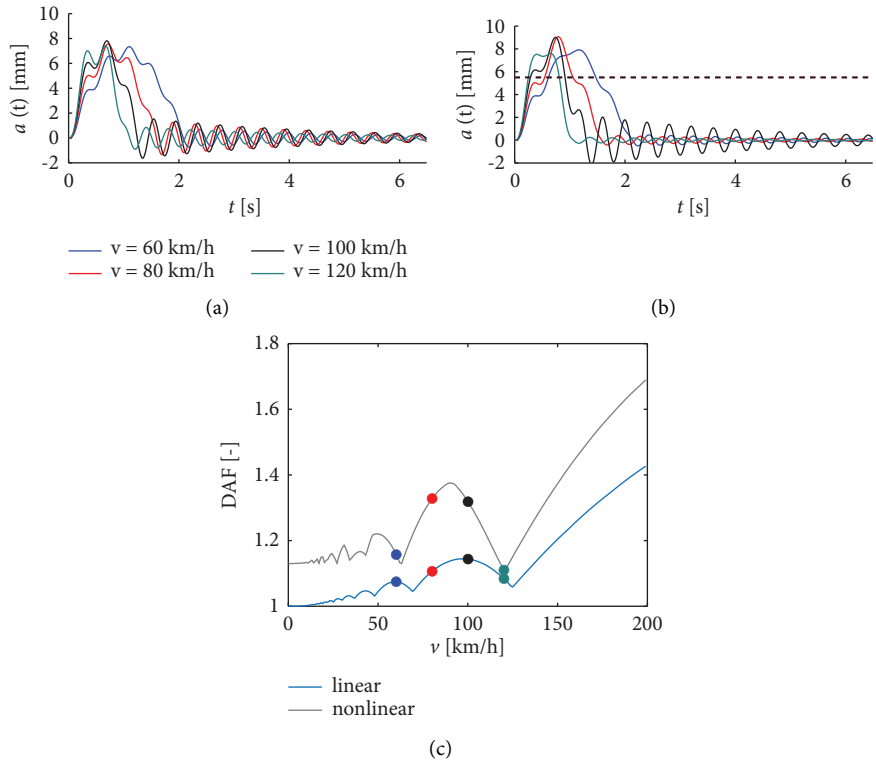

FIGURE 15: Response time histories of the deflection experienced by (a) linear and (b) nonlinear systems under the different vehicle velocities; (c) dynamic amplification factors (DAFs) for a wide range of vehicle velocities (coloured circles identifying analysed cases).

case, as already acknowledged in the technical literature [21]. In particular, the system properties are kept fixed at the reference values ($k_1/k_0 = 0.60$, $a^* = 5.5$ mm), while the following set of vehicle velocities are analysed: 60 km/h ($S = 0.0952$), 80 km/h ($S = 0.1270$), 100 km/h ($S = 0.1587$), and 120 km/h ($S = 0.1905$). The moving load with $P = 440$ kN is considered.

With the aim of shedding light on the influence of this parameter on the bridge response, a preliminary brief comparison is proposed in Figure 15, where the response time histories of the midspan deflection experienced by the system assumed linear elastic (Figure 15(a)) and nonlinear elastic (Figure 15(b)) are shown; it can be noted as a dynamic response is still observable for all the range of vehicle velocities (thus S ratios) investigated. The attained maximum displacements do not rise proportionally with the velocity, and the trend can be better appreciated and understood from Figure 15(c), where the dynamic amplification factors (DAF, i.e., the ratio of the dynamic to the static response) for a wide range of vehicle velocities are plotted (analysed velocities highlighted by coloured circles). For the sake of completeness, DAFs are also computed and shown for the case of the nonlinear system; the static value used for the normalization is the one stemming from the linear system response, so that the entity of the amplification produced by the assumed level of nonlinearity can also be appreciated.

In Figure 16, the frequency-amplitude correlation chart is presented for all the analysed cases, and the conditional PDFs of the instantaneous frequency are provided in Figure 17. The outcomes show how the cases associated with higher DAFs (80 km/h and 100 km/h) allow attaining higher displacements helping to stabilize the instantaneous frequency values around the reduced frequency value ω_1. Transition from ω_0 to ω_1 starts occurring, in all cases, at displacements higher than the threshold $a^* = 5.5$ mm, with the vehicle velocity not having influence on this aspect. In conclusion, it is worth noting how the velocities producing clearer and more stable frequency modifications falls within the range of speeds at which heavy trucks usually travel (in particular, the case of 80 km/h).

4.5. Influence of Vehicle Weight. In order to stress the key role played by the heavy traffic in the proposed methodology, the response under three travelling vehicles with different weights is compared: 60 kN, 260 kN, and 440 kN, all moving at a constant velocity equal to 80 km/h.

In Figure 18(a), the response time histories are compared, and it can be seen as the first elastic limit is only exceeded for the heavy travelling load. In Figure 18(b), the frequency-amplitude correlation chart is presented, and the PDFs of the instantaneous frequency conditional to the response amplitudes are provided in Figure 19 (charts from *a* to *f*). From the inspections of these results, it can be observed that the weights of the light and intermediate vehicles are not sufficiently high to produce a nonlinear response of the bridge; as a consequence, the corresponding instantaneous frequency distributions remain unchanged

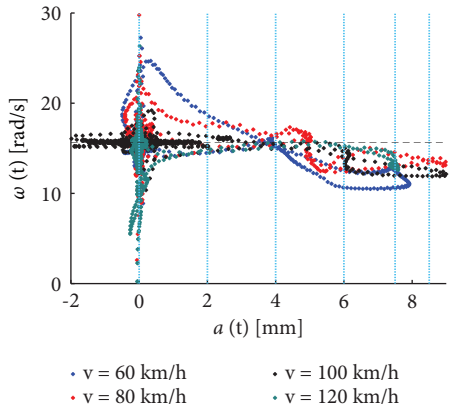

FIGURE 16: Frequency-amplitude correlation chart for different vehicle velocities.

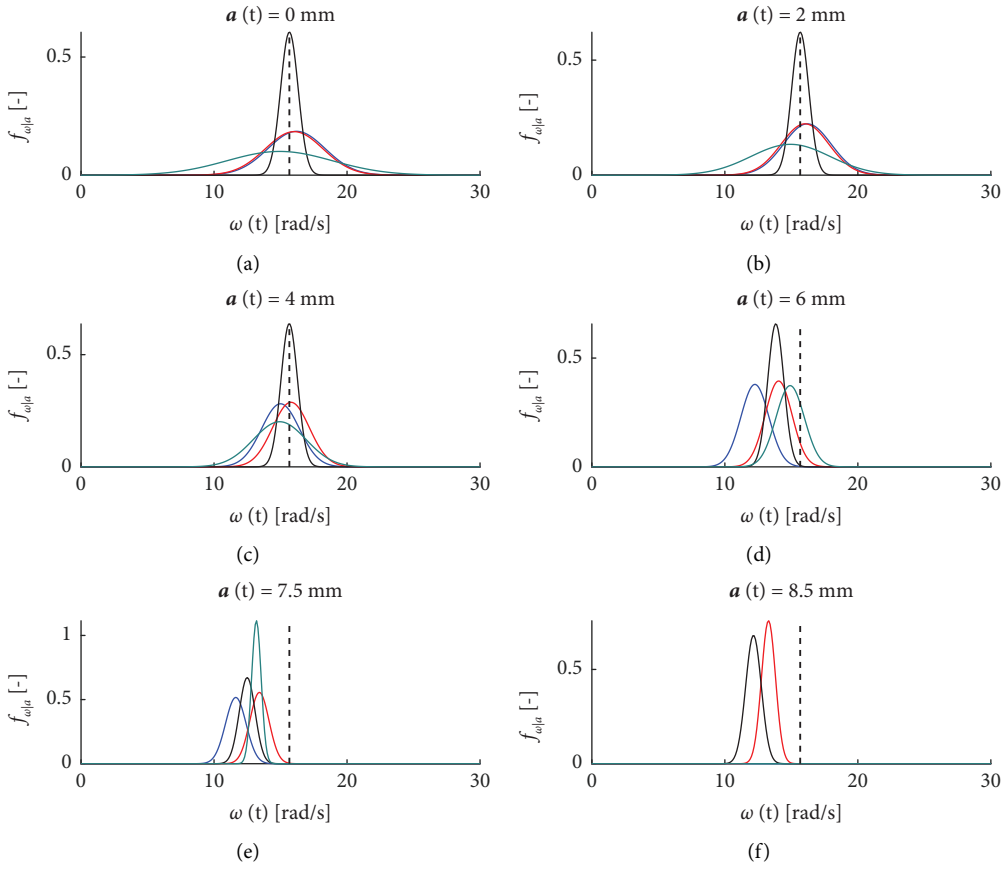

FIGURE 17: Instantaneous frequency distributions conditional to increasing levels of the response amplitude for different vehicle velocities: 60 km/h (blue), 80 km/h (red), 100 km/h (black), and 120 km/h (green).

with the mean fixed at the reference value ω_0 within the whole range of displacement amplitudes (there is just a slight reduction of the dispersion with the response amplitudes).

4.6. Influence of Consecutive Moving Loads (Traffic Sequences). The parametric investigation is concluded with the analysis of more realistic traffic sequences characterised by the passage of multiple vehicles with different mass, velocity, and interarrival time. In particular, the three sequences S1, S2, and S3 described in Table 1 are considered, which differ from each other by the number of 440 kN heavy vehicles (1 in S1, 2 in S2, and 3 in S3).

The response deflection time histories produced by the three sequences are shown in Figure 20(a) (first elastic threshold exceeded by the passage of heavy vehicles only). In Figure 20(b), the frequency-amplitude correlation chart is presented, and the PDFs of the instantaneous frequency conditional to four amplitude levels are provided in Figure 21.

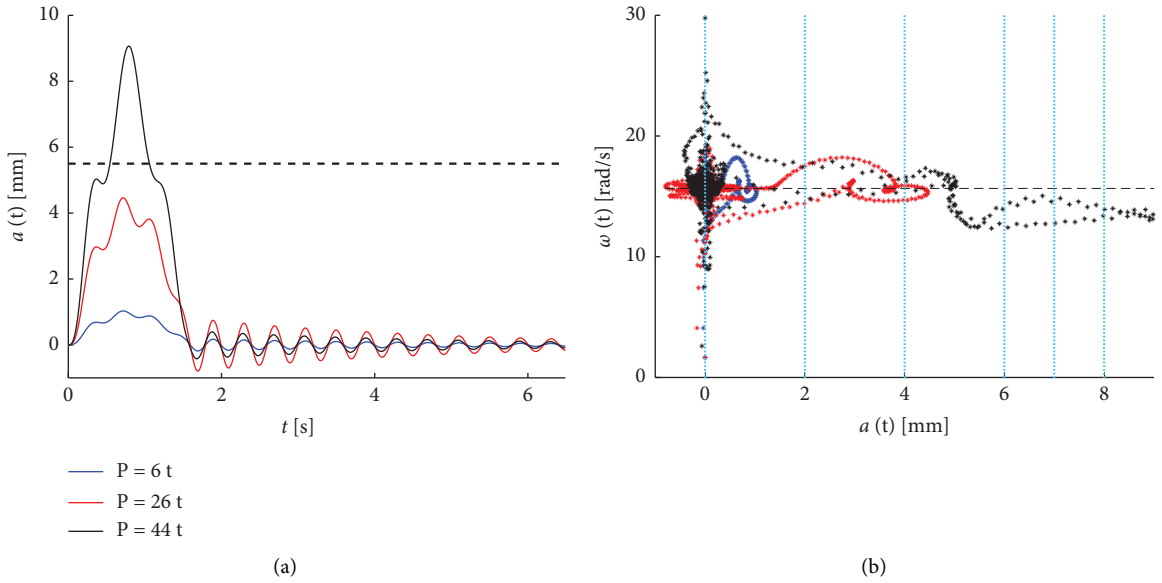

FIGURE 18: (a) Bridge deflection time series and (b) frequency-amplitude correlation chart for travelling loads with different weight.

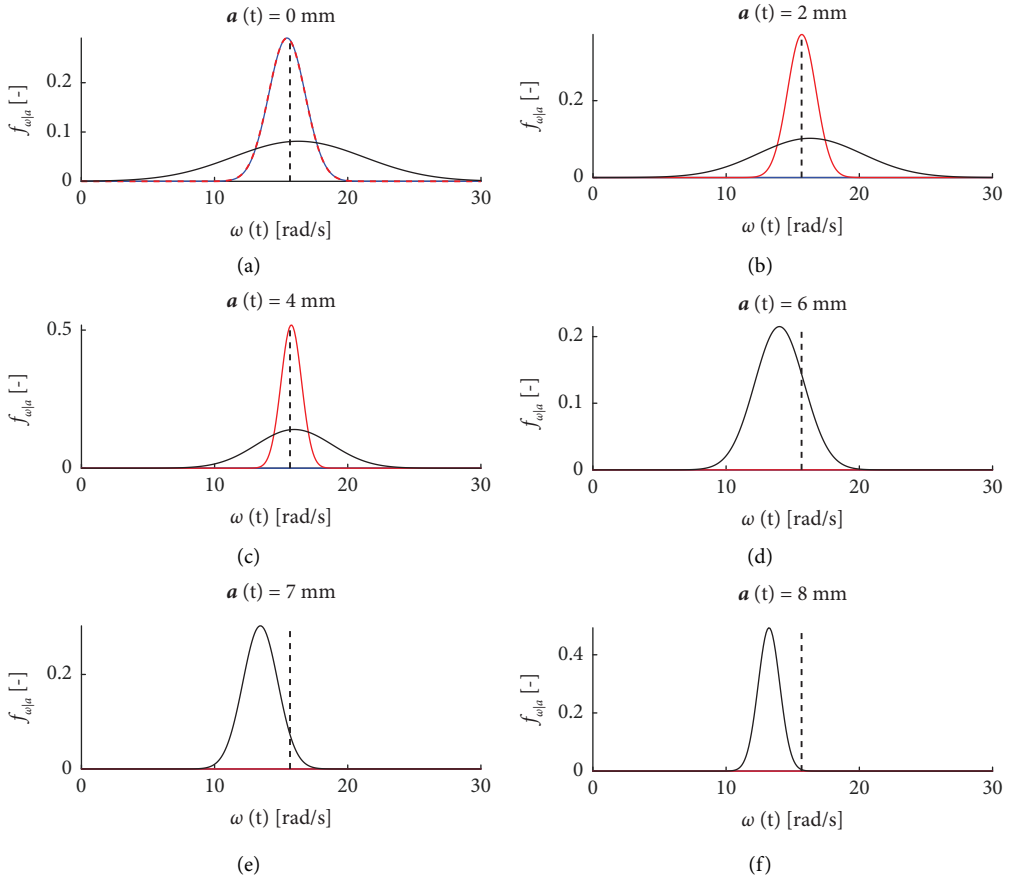

FIGURE 19: Instantaneous frequency distributions conditional to increasing levels of the amplitude for light (blue), intermediate (red), and heavy (black) moving loads.

Results show how all the three sequences carry the same relevant information on the system nonlinearity and the presence of lighter vehicles within the same time window does not jeopardise the observability of the phenomenon. On the other hand, the presence of more than one heavy vehicle might make the data more robust, helping to identify

Table 1: Features of the considered traffic sequences.

Traffic sequence	Load 1		Load 2		Load 3		Load 4	
	P (kN)	v (km/h)	P (kN)	v (km/h)	P (kN)	v (km/h)	P (kN)	v (km/h)
S1	440	60	60	130	260	90	90	100
S2	440	60	440	70	260	90	90	100
S3	440	60	440	70	260	90	440	80

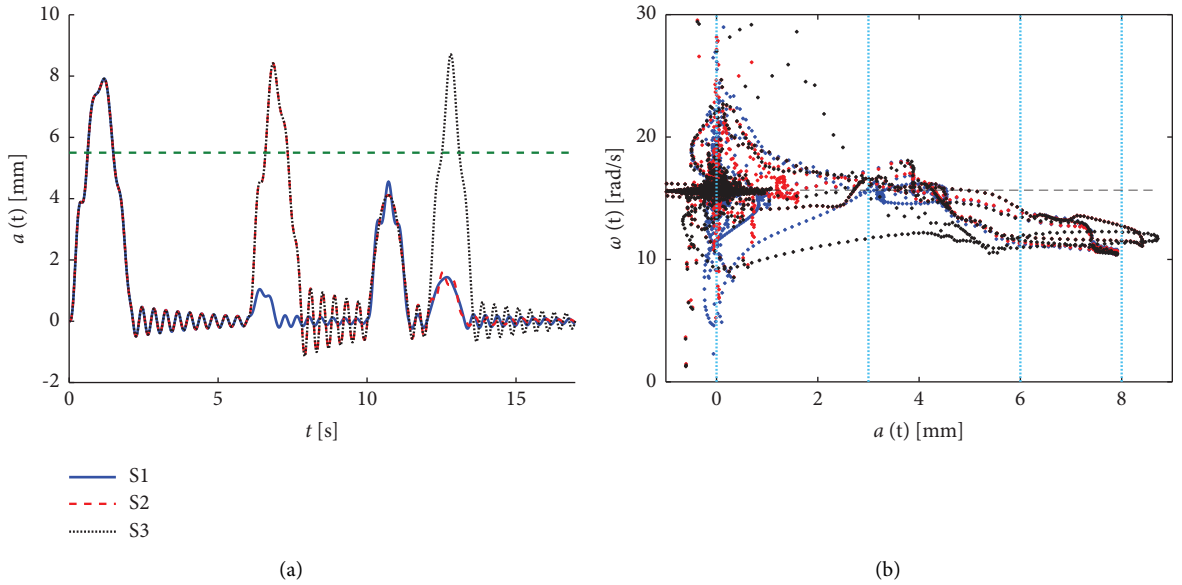

Figure 20: (a) Bridge deflection time series and (b) frequency-amplitude correlation chart for three different traffic sequences.

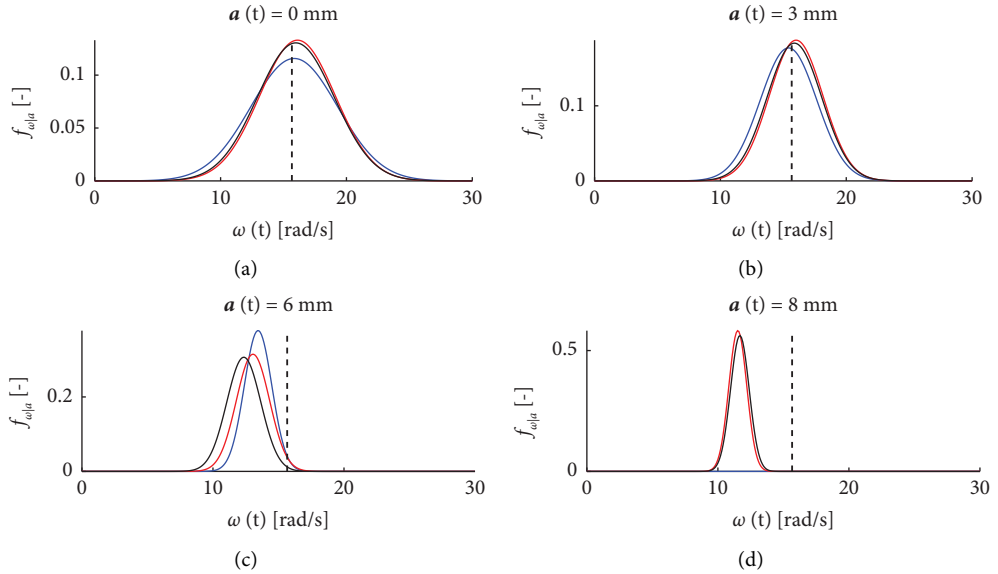

Figure 21: Instantaneous frequency distributions conditional to increasing levels of the response amplitude; comparison of three different traffic sequences.

the response deviation from linearity, so data recording over a sufficiently long time interval is recommended in order to catch multiple truck passages.

5. Conclusions

A novel methodology was proposed to identify the nonlinear response and prestressing level of post-tensioned r.c. bridges. The analysis is based on the input produced by the heavy traffic travelling on the structure during its operational conditions. The abilities of the Hilbert–Huang Transform (HHT) to extract the instantaneous property of the dynamic response were exploited, and a novel procedure to recover the nonlinear elastic response of these systems was presented and investigated through theoretical applications on simple dynamic systems.

The main conclusions can be summarised through the following points:

(i) A frequency-amplitude correlation chart was proposed as a visual tool to retrieve useful information on the nonlinear relationship between displacement and tangent stiffness.

(ii) With the aim of denoising and eliminating spurious contributions introduced by the local nature of the information extracted through the Hilbert spectral analysis, a probabilistic model was proposed for the result interpretation through which the probability distribution of the instantaneous natural frequencies conditional to different levels of the response amplitude is provided. The model has been inferred by the maximum likelihood method, and satisfactory results have been obtained using a normal Gaussian PDF with simple variation laws for the median and variance.

(iii) The probabilistic model proved to be a useful tool to highlight variations in the trend and to identify potential anomalies that could result otherwise hidden by the noisy data reported in the frequency-amplitude correlation charts.

(iv) According to the outcomes of the parametric analysis, the methodology revealed effective in identifying nonlinear trends in the system response, also in case of the low level of nonlinearity. In particular, the analysis method makes it possible to separately identify both the two main characteristic parameters of the nonlinear behaviour: the threshold of the stiffness variation related to the intensity of the prestressing force and the slope of the second branch related to the girder properties.

(v) Furthermore, the method demonstrated to be effective in the range travelling load velocity of practical interest.

The study outcomes and the associated relevance call for further investigations, such as: (i) application of the proposed HHT-based methodology to real bridges using data recorded from structural monitoring campaign, in order to test and strengthen the theoretical results; (ii) alternative and potentially more effective methods for pattern recognition should be explored for the data analysis and anomaly detection; (iii) higher modes should be included in the methodology, given that they may not reveal negligible in other more complex static schemes.

Data Availability

Data are available on request by contacting the corresponding author.

Conflicts of Interest

The authors declare that they have no conflicts of interest.

Acknowledgments

This research was funded in part by the European Union, FSE, Pon Research and Innovation 2014–2020. Moreover, this work was financially supported by FABRE – Research Consortium for the evaluation and monitoring of bridges, viaducts, and other structures – through funds for basic research on "multilevel safety analysis and monitoring of existing bridges."

References

[1] COST, "COST 345 procedures for the assessment of Highway structures," Final Report, European Commission, Brussels, Belgium, 2004.

[2] L. Minnucci, F. Scozzese, S. Carbonari, F. Gara, and A. Dall'Asta, "Innovative fragility-based method for failure mechanisms and damage extension analysis of bridges," *Infrastructure*, vol. 7, no. 9, p. 122, 2022.

[3] B. Borzi, P. Ceresa, P. Franchin, F. Noto, G. M. Calvi, and P. E. Pinto, "Seismic vulnerability of the Italian roadway bridge stock," *Earthquake Spectra*, vol. 31, no. 4, pp. 2137–2161, 2015.

[4] Federal Highway Administration, "HRT-13-028: Guidelines for sampling, assessing, and restoring defective grout in prestressed concrete bridge post-tensioning duts," Technical Report, Federal Highway Administration, Washington, DC, USA, 2013.

[5] Highways England, *CS 465– Management of Post-Tensioned Concrete Bridges*, Highways England, Guildford, UK, 2020.

[6] Highways England, *CS 464–Non-Destructive Testing on Highways Structures*, Highways England, Guildford, UK, 2020.

[7] Ministero delle Infrastrutture e della Mobilità Sostenibili, "Linee guida per la classificazione e gestione del rischio, la valutazione della sicurezza ed il monitoraggio dei ponti esistenti. (22A04700) (GU Serie Generale n.196 del 23-08-2022)," 2022, https://www.gazzettaufficiale.it/eli/id/2022/08/23/22A04700/sg.

[8] L. Wang, T. Li, L. Dai, W. Chen, and K. Huang, "Corrosion morphology and mechanical behavior of corroded prestressing strands," *Journal of Advanced Concrete Technology*, vol. 18, no. 10, pp. 545–557, 2020.

[9] L. Wang, *Strand Corrosion in Prestressed concrete Structures*, Springer Nature Singapore Pte Ltd, Singapore, 2023.

[10] W. Podolny, "Corrosion of prestressing steel and its mitigation," *PCI Journal*, vol. 37, 1992.

[11] N. R. Hewson, *Prestressed concrete Bridges: Design and Construction*, Thomas Telford, England, UK, 2003.

[12] T. García-Segura, V. Yepes, and D. M. Frangopol, "Multi-objective design of post-tensioned concrete road bridges using artificial neural networks," *Structural and Multidisciplinary Optimization*, vol. 56, no. 1, pp. 139–150, 2017.
[13] R. Brincker and C. Ventura, *Introduction to Operational Modal Analysis*, John Wiley & Sons, Hoboken, NJ, USA, 2015.
[14] M. Saiidi, B. Douglas, and S. Feng, "Prestress force effect on vibration frequency of concrete bridges," *Journal of Structural Engineering*, vol. 120, no. 7, pp. 2233–2241, 1994.
[15] A. Dall'Asta and G. Leoni, "Vibrations of beams prestressed by internal frictionless cables," *Journal of Sound and Vibration*, vol. 222, no. 1, pp. 1–18, 1999.
[16] A. Dall'Asta, "Dynamics of elastic bodies prestressed by internal slipping cables," *International Journal of Solids and Structures*, vol. 37, no. 25, pp. 3421–3438, 2000.
[17] D. Noble, M. Nogal, A. O'Connor, and V. Pakrashi, "The effect of prestress force magnitude and eccentricity on the natural bending frequencies of uncracked prestressed concrete beams," *Journal of Sound and Vibration*, vol. 365, pp. 22–44, 2016.
[18] E. Hamed and Y. Frostig, "Natural frequencies of bonded and unbonded prestressed beams-prestress force effects," *Journal of Sound and Vibration*, vol. 295, no. 1-2, pp. 28–39, 2006.
[19] N. E. Huang, *Hilbert-huang Transform and its Applications*, vol. 16, World Scientific, Singapore, 2014.
[20] B. Chen, S. L. Zhao, and P. Y. Li, "Application of hilbert-huang transform in structural health monitoring: a state-of-the-art review," *Mathematical Problems in Engineering*, vol. 2014, no. 7, Article ID 317954, 22 pages, 2014.
[21] Y. B. Yang, J. D. Yau, Z. Yao, and Y. S. Wu, *Vehicle-bridge Interaction Dynamics: With Applications to High-Speed Railways*, World Scientific, Singapore, 2004.
[22] K. V. Nguyen, "Comparison studies of open and breathing crack detections of a beam-like bridge subjected to a moving vehicle," *Engineering Structures*, vol. 51, pp. 306–314, 2013.
[23] A. Gomez-Cabrera and P. J. Escamilla-Ambrosio, "Review of machine-learning techniques applied to structural health monitoring systems for building and bridge structures," *Applied Sciences*, vol. 12, no. 21, Article ID 10754, 2022.
[24] B. Bozyigit and S. Acikgoz, "Dynamic amplification in masonry arch railway bridges," in *Structures*, vol. 45, pp. 1717–1728, Elsevier, Amsterdam, Netherlands, 2022.
[25] A. Ghannadiasl and S. Khodapanah Ajirlou, "Dynamic analysis of multiple cracked Timoshenko beam under moving load–analytical method," *Journal of Vibration and Control*, vol. 28, no. 3-4, pp. 379–395, 2022.
[26] B. Bozyigit, "Dynamic response of damaged rigid-frame bridges subjected to moving loads using analytical based formulations," *Engineering Computations*, vol. 40, no. 4, pp. 793–822, 2023.
[27] M. Ahmadi and A. Nikkhoo, "Utilization of characteristic polynomials in vibration analysis of non-uniform beams under a moving mass excitation," *Applied Mathematical Modelling*, vol. 38, no. 7-8, pp. 2130–2140, 2014.
[28] F. Feng, F. Huang, W. Wen, Z. Liu, and X. Liu, "Evaluating the dynamic response of the bridge-vehicle system considering random road roughness based on the moment method," *Advances in Civil Engineering*, vol. 2021, Article ID 9923592, 12 pages, 2021.
[29] S. P. Timoshenko, "CV. On the forced vibrations of bridges," *The London, Edinburgh and Dublin Philosophical Magazine and Journal of Science*, vol. 43, no. 257, pp. 1018-1019, 1922.
[30] H. H. Jeffcott, "VI. On the vibration of beams under the action of moving loads," *The London, Edinburgh and Dublin Philosophical Magazine and Journal of Science*, vol. 8, no. 48, pp. 66–97, 1929.
[31] A. N. Lowan, "LIV. On transverse oscillations of beams under the action of moving variable loads," *The London, Edinburgh and Dublin Philosophical Magazine and Journal of Science*, vol. 19, no. 127, pp. 708–715, 1935.
[32] L. Frýba, *Vibration of Solids and Structures under Moving Loads*, Thomas Telford, England, UK, 1999.
[33] J. T. Oden and J. N. Reddy, *Variational Methods in Theoretical Mechanics*, Springer-Verlag, Berlin, Germany, 1976.
[34] A. Dall'Asta and G. Menditto, "Perturbed motion of visco-elastic columns: a variational approach," *International Journal of Solids and Structures*, vol. 30, 1992.
[35] N. E. Huang, Z. Shen, S. R. Long et al., "The empirical mode decomposition and the Hilbert spectrum for nonlinear and non-stationary time series analysis," *Proceedings of the Royal Society Series A: Mathematical, Physical and Engineering Sciences*, vol. 454, pp. 903–995, 1998.
[36] L. Cohen, *Time-frequency Analysis*, vol. 778, Prentice-Hall, New Jersey, NJ, USA, 1995.
[37] G. Kerschen, A. F. Vakakis, Y. S. Lee, D. M. McFarland, and L. A. Bergman, "Toward a fundamental understanding of the Hilbert-Huang transform in nonlinear structural dynamics," *Journal of Vibration and Control*, vol. 14, no. 1-2, pp. 77–105, 2008.
[38] D. Lallemant, A. Kiremidjian, and H. Burton, "Statistical procedures for developing earthquake damage fragility curves," *Earthquake Engineering and Structural Dynamics*, vol. 44, pp. 1373–1389, 2015.
[39] M. Morici, C. Canuti, and A. Dall'Asta, "Empirical predictive model for seismic damage of historical churches," *Bulletin of Earthquake Engineering*, vol. 18, pp. 6015–6037, 2020.
[40] L. Gioiella, M. Morici, and A. Dall'Asta, "Empirical predictive model for seismic damage and economic losses of Italian school building heritage," *International Journal of Disaster Risk Reduction*, vol. 91, 2023.
[41] H. Munthe-Kaas, "High order Runge-Kutta methods on manifolds," *Applied Numerical Mathematics*, vol. 29, no. 1, pp. 115–127, 1999.
[42] The MathWorks Inc, *MATLAB Version: 9.13.0 (R2022b)*, The MathWorks Inc, Natick, MA, USA, 2022.
[43] G. De Ceuster, T. Breemersch, B. Van Herbruggen et al., "Effects of adapting the rules on weights and dimensions of heavy commercial vehicles as established within Directive 96/53/EC," Final report, European Commission, Brussels, Belgium, 2008.